

## A COMPUTER SIMULATION OF A POTENTIAL DERIVED FROM THE GAY-BERNE POTENTIAL FOR LATTICE MODEL

Habtamu Zewdie

Department of Chemistry, Addis Ababa University, P.O. Box 1176, Addis Ababa, Ethiopia

(Received February 28, 2000; revised March 24, 2000)

**ABSTRACT.** The lattice model of elongated molecules interacting via a potential derived from the Gay-Berne pair potential is proposed. We made a systematic study of the effect of varying the molecular elongation and intermolecular vector orientation dependence of the pair potential on the thermodynamic as well as the structural properties of liquid crystals. A Monte Carlo simulations of molecules placed at the site of a simple cubic lattice and interacting via the modified Gay-Berne potential with its nearest neighbours is performed. The internal energy, heat capacity, angular pair correlation function and scalar order parameter are obtained. The results are compared against predictions of molecular field theory, experimental results and that of other related simulations wherever possible. It is shown that for more elongated molecules the nematic-isotropic transition becomes stronger first order transition. For a given molecular elongation as the intermolecular vector orientation dependence becomes larger the nematic-isotropic transition becomes a stronger first order transition as measured by the rate of change of the order parameter and the divergence of the heat capacity. Scaling the potential well seems to have dramatic change on the effect of the potential well anisotropy on trends of nematic-isotropic transition temperature and divergence of the heat capacity. It is shown that the behaviour of many nematics can be described by proposed model with the elongation ratio of molecules and potential well anisotropy ranging from 3 to 5.

### INTRODUCTION

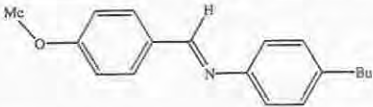
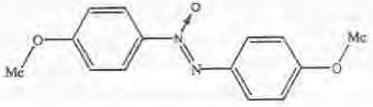

Ordinary fluids are isotropic in nature: they appear optically, magnetically, electrically, etc. to be the same from any perspective. Although the molecules which comprise the fluid are generally anisotropic in shape, this anisotropy generally plays little role in anisotropic macroscopic behaviour. Nevertheless, there exists a large class of highly anisotropic molecules which gives rise to unusual, fascinating, and potentially technologically relevant behaviour. There are many interesting candidates for study, including polymers, micelles, micro emulsions, and materials of biological significance, such as DNA and membrane. Our primary effort centers on liquid crystals [1].

Liquid crystals are composed of moderate size organic molecules (length  $\sigma_l = 20-30 \text{ \AA}$  and width  $\sigma_w = 5-6 \text{ \AA}$  with length to width ratio of  $\sigma_l/\sigma_w = 3-6$ ) which tend to be elongated and shaped like a cigar. Typical structures of well studied mesogens and a simplified model of them which is commonly used in theory and computer simulation and known to mimic a variety of mesophases are given in Table 1. Although the literature is full of a variety of other, highly exotic shapes as well. Because of their elongated shape, under appropriate conditions the molecules can exhibit orientational order, such that all the axes on the average line up in a particular direction which is known as the director and designated by  $\hat{n}$ . In consequence, the bulk order has profound influence on the way the material behaves optically, magnetically, and electrically [2,3].

The main characteristic of liquid crystals, and what makes them particularly difficult to

study and simulate, is the existence of orientational and possibly positional order and the presence of transitions between phases where some of these order parameters vanish. A transition of particular importance is the nematic-isotropic one, where the orientational order goes to zero. The transition is experimentally of a weak first-order character.

Table 1. Molecular structures of typical mesogenic molecules, a simplified model and their transitional properties.

Typical mesogenic molecules and a simplified model	$\sigma_v/\sigma_l$	$T_{NI}/C^0$	$P_2^{NI}$
 <p>4-Methoxybenzylidene-4'-n-butylaniline (MBBA)</p>	3	48	0.28
 <p>4,4'-Dimethoxyazoxybenzene (PAA)</p>	4	136	0.38
 <p>Prolate ellipsoid</p>			

The understanding of liquid crystals at the molecular level via computer simulation is dictated by the availability of suitable potential models. Realistic atom-atom potential models of liquid crystals are available, but the associated simulations require a large amount of computer resources [4-6]. However, significant progress in understanding the liquid-crystalline state has been made by simulating a range of simplified potential models such as lattice models [7-11], hard spherocylinder and ellipsoidal particles [12-13], soft-core [14-15], and single-site model potentials [16-19]. Thus while idealized models may be used to study quite general, fundamental properties of mesophases, the modelling of specific liquid crystal systems in a realistic way remains a great challenge. Progress continues to be made on both these fronts.

To favour orientational ordering the intermolecular interaction in nematogens have to be sufficiently anisotropic. In general they consist of both long-range anisotropic interactions and short-ranged repulsive ones, which complicates theoretical description of such systems. It is evident that increasing of the system size together with the use of realistic potentials become very time consuming. For this reason models of the same level of simplicity as Lebwohl-Lasher [7] model seemed to be still useful for investigation of phase transitions in anisotropic systems [20-21].

Lattice models are known to play an important role in the theory of phase transitions. This has been recognized for spin systems and for systems mimicking the orientational phase transition found in mesophases [7,22]. In the liquid crystal field one of the most popular models is that originally due to Lebwohl and Lasher [7-11, 23-25], where particles are placed

on a simple cubic lattice and allowed to interact with the pair potential

$$U_{ij} = -\epsilon_{ij} P_2(\hat{u}_i, \hat{u}_j) \quad (1)$$

Here  $\epsilon_{ij}$  is a parameter expressing the strength of the attractive interaction. It is a positive constant,  $\epsilon_{ij}$  for nearest neighbour particles  $i$  and  $j$  and zero otherwise.  $\hat{u}_i$  and  $\hat{u}_j$  are unit axial vectors defining the orientations of molecules  $i$  and  $j$  in some arbitrary space fixed frame.

The Lebwohl-Lasher (LL) model is capable of giving satisfactory quantitative description of the nematic-isotropic transition in the liquid crystal materials [19-20]. However, the temperature dependence of the order parameter, the transition temperature, and the values for the latent heat  $\Delta \bar{U}_{NI}^*$  as well as the nematic order parameter at the transition  $\bar{P}_2^{NI}$  given by LL model are fixed and cannot cover the entire interval of typical experimental values for real nematic [25]. To bring more flexibility into the lattice model several attempts have been made to introduce additional parameters connected with the details of the intermolecular interaction. The intermolecular vector orientation dependence of the pair potential in terms of the unit vectors  $\hat{u}_1$ ,  $\hat{u}_2$ , and  $\hat{r}$  describing the orientations of the two linear particles and the intermolecular vector was given as [26]

$$U(\hat{u}_1, \hat{u}_2, \hat{r}) = \gamma \epsilon_0 \{ 1 - (3/2)(\hat{u}_1, \hat{r})^2 - (3/2)(\hat{u}_2, \hat{r})^2 \} + (3/2)\gamma^2 \epsilon_0 \{ (\hat{u}_1, \hat{r})^2 + (\hat{u}_2, \hat{r})^2 - 9(\hat{u}_1, \hat{r})^2 (\hat{u}_2, \hat{r})^2 + 6(\hat{u}_1, \hat{r})(\hat{u}_2, \hat{r})(\hat{u}_1, \hat{u}_2) - (\hat{u}_1, \hat{u}_2)^2 \} \quad (2)$$

where  $\gamma = (\alpha_{\parallel} - \alpha_{\perp}) / (\alpha_{\parallel} + \alpha_{\perp})$  is the relative anisotropy in the polarizability. For this dispersion potential the well depth when the molecules are parallel to each other and to the intermolecular vector (end-to-end configuration) is given by  $\epsilon_e = -2\gamma \epsilon_0 - (3/2)\gamma^2 \epsilon_0$  and when the molecules are perpendicular to the intermolecular vector but still parallel to each other (side-by-side configuration) the potential well depth is given by  $\epsilon_s = \gamma \epsilon_0 - (3/2)\gamma^2 \epsilon_0$ . For any positive value of  $\gamma$  we always find  $\epsilon_e < \epsilon_s$ . Such potentials are more relevant to the study of discotic systems rather than rod-like systems [18-19]. For rod-like systems we always find  $\epsilon_e > \epsilon_s$ . For the sake of brevity we shall refer to this potential as HLR potential in future discussions. The effect of molecular elongation was investigated by modifying the overlap potential model of Berne and Pechukas [16, 20]. This will be described in detail in the following section.

We suppose that the dependence of the pair potential both on the intermolecular vector orientation and the molecular elongation and its influence on the properties of a nematic can be better studied by modifying the more realistic Gay-Berne model potential (GB) [17]. In the case where we retain the lattice restriction to the centre of mass of the interacting particles, the translational dependent part of the potential will be lost, and only the essential angular part will remain. This will retain the long range intermolecular interaction with the dependence of the potential on the parameters of molecular elongation and intermolecular vector orientation. We shall refer to this potential as GBA in the future discussions.

To explore the value of the GBA model potential for studies of liquid crystals, we have carried out a detailed Monte Carlo simulation. The range of stability and the nature of the nematic-isotropic transition have been determined. The influence of intermolecular vector on the structure and thermodynamic properties of the phases is explored. In the following section the model potential will be discussed followed by the details of the computer simulation. The results of the simulation will be given and discussed. The final section contains the conclusions.

## THE MODEL POTENTIAL

The GB potential model has proved to be valuable for computer simulation studies of the liquid-crystalline state [27-33]. It is a single-site model potential which possesses both the short-range repulsion and long-range attraction. It has the shifted Lennard-Jones form with strength and range parameters dependent on the orientations of the molecules and the intermolecular vector. The form of the pair potential is given as

$$U(\hat{u}_i, \hat{u}_j, \hat{r}) = 4\epsilon(\hat{u}_i, \hat{u}_j, \hat{r}) \left[ \left( \frac{\sigma_0}{r - \sigma(\hat{u}_i, \hat{u}_j, \hat{r}) + \sigma_0} \right)^{12} - \left( \frac{\sigma_0}{r - \sigma(\hat{u}_i, \hat{u}_j, \hat{r}) + \sigma_0} \right)^6 \right] \quad (3)$$

The range parameter of the potential,  $\sigma(\hat{u}_i, \hat{u}_j, \hat{r})$  is given as

$$\sigma(\hat{u}_i, \hat{u}_j, \hat{r}) = \sigma_0 \left[ 1 - \frac{\chi}{2} \left( \frac{(\hat{u}_i \cdot \hat{r} + \hat{u}_j \cdot \hat{r})^2 + (\hat{u}_i \cdot \hat{r} - \hat{u}_j \cdot \hat{r})^2}{1 + \chi(\hat{u}_i \cdot \hat{u}_j)} + \frac{(\hat{u}_i \cdot \hat{r} - \hat{u}_j \cdot \hat{r})^2}{1 - \chi(\hat{u}_i \cdot \hat{u}_j)} \right) \right]^{-1/2} \quad (4)$$

Here  $\chi = (\kappa^2 - 1)/(\kappa^2 + 1)$  is determined by the shape anisotropy of the ellipsoidal Gaussian  $\kappa$  defined as  $\kappa = \sigma_{\parallel}/\sigma_{\perp}$ .  $\sigma_{\parallel}$  and  $\sigma_{\perp}$  are the major and minor axes of the ellipsoid where  $\sigma_0$  is a length scale parameter which reflects the molecular size. The strength parameter  $\epsilon(\hat{u}_i, \hat{u}_j, \hat{r})$  is given as

$$\epsilon(\hat{u}_i, \hat{u}_j, \hat{r}) = \epsilon_0 \epsilon^{\nu}(\hat{u}_i, \hat{u}_j) \epsilon^{\mu}(\hat{u}_i, \hat{u}_j, \hat{r}) \quad (5)$$

where  $\epsilon_0$  is the well depth for cross-configuration which is used for scaling energy and other related thermodynamic properties.  $\epsilon(\hat{u}_i, \hat{u}_j)$  is given as

$$\epsilon(\hat{u}_i, \hat{u}_j) = [1 - \chi^2(\hat{u}_i, \hat{u}_j)^2]^{-1/2} \quad (6)$$

and  $\epsilon^{\nu}(\hat{u}_i, \hat{u}_j, \hat{r})$  is assumed to have the form  $\sigma_0^2/\sigma^2(\hat{u}_i, \hat{u}_j, \hat{r})$  with a new anisotropy parameter defined as  $\chi' = (\kappa'^{1/\mu} - 1)/(\kappa'^{1/\mu} + 1)$ . The new potential anisotropy parameter  $\kappa'$  is defined as  $\kappa' = \epsilon_s/\epsilon_e$  where  $\epsilon_s$  is the side-by-side and  $\epsilon_e$  end-to-end well depths, respectively. The explicit form of  $\epsilon^{\nu}(\hat{u}_i, \hat{u}_j, \hat{r})$  is given as

$$\epsilon^{\nu}(\hat{u}_i, \hat{u}_j, \hat{r}) = 1 - \frac{\chi'}{2} \left[ \frac{(\hat{u}_i \cdot \hat{r} + \hat{u}_j \cdot \hat{r})^2 + (\hat{u}_i \cdot \hat{r} - \hat{u}_j \cdot \hat{r})^2}{1 + \chi'(\hat{u}_i \cdot \hat{u}_j)} + \frac{(\hat{u}_i \cdot \hat{r} - \hat{u}_j \cdot \hat{r})^2}{1 - \chi'(\hat{u}_i \cdot \hat{u}_j)} \right] \quad (7)$$

The two parameters  $\mu$  and  $\nu$  in the well depth function take different sets of values without affecting the relative well depths for the side-by-side and end-to-end configurations. However, if  $\mu \leq \nu$  the potential has more desirable features; the side-by-side configuration is more stable than the cross and the T-configurations, and the end-to-end configuration is more stable than the T-configuration.

If we restrict the centre of mass of particle to lattice sites we only need part of the GB potential which could be written as

$$U(\hat{u}_i, \hat{u}_j, \hat{r}) = -\epsilon(\hat{u}_i, \hat{u}_j, \hat{r}) = -\epsilon_0 \epsilon^{\nu}(\hat{u}_i, \hat{u}_j) \epsilon^{\mu}(\hat{u}_i, \hat{u}_j, \hat{r}) \quad (8)$$

which we shall call GBA for the sake of brevity. In order to be able to make a direct comparison with the results of the LL model and that of other related simulations we will

scale this modified GB potential in such a way that the limiting value of the potential for the side-by-side configuration coincides with the Maier-Saupe type potential. The  $\epsilon'(\hat{u}_i, \hat{u}_j, \hat{r})$  part is already scaled. We are now left with the  $\epsilon(\hat{u}_i, \hat{u}_j)$  part. For this we follow the scaling procedure given in Ref. [20] and obtain an expression for the scaled  $\epsilon_N(\hat{u}_i, \hat{u}_j)$  as

$$\epsilon_N(\hat{u}_i, \hat{u}_j) = \frac{1}{2} \left[ \frac{6\kappa}{(\kappa-1)^2} \left( \frac{1}{\sqrt{1-\chi^2(\hat{u}_i, \hat{u}_j)^2}} - 1 \right) - 1 \right] \quad (9)$$

In the limit of small anisotropy  $\chi \ll 1$  the exact form of the Lebwohl-Lasher potential given by equation (1) is reproduced. As  $\kappa$  increases the potential becomes more anisotropic. The scaled GBA potential which we shall refer to it as GBAN potential is given as

$$U(\hat{u}_i, \hat{u}_j, \hat{r}) = -\epsilon_0 \epsilon_N^v(\hat{u}_i, \hat{u}_j) \epsilon'^{\mu}(\hat{u}_i, \hat{u}_j, \hat{r}) \quad (10)$$

where  $\epsilon'$  and  $\epsilon_N$  are given by equations (7) and (9), respectively. The GB potential requires four parameters to be explicitly selected:  $\kappa = \sigma_{\parallel}/\sigma_{\perp}$  and  $\kappa' = \epsilon_s/\epsilon_e$  which, respectively, define the shape and well-depth anisotropies, and  $\mu$  and  $\nu$ , which adjust the relative strength of various intermolecular interactions.

Next we shall explore in detail the dependence of the pair potentials GBAN and GBA on the four parameters  $\kappa$ ,  $\kappa'$ ,  $\mu$  and  $\nu$  and compare them against LL and BPAN model potentials.

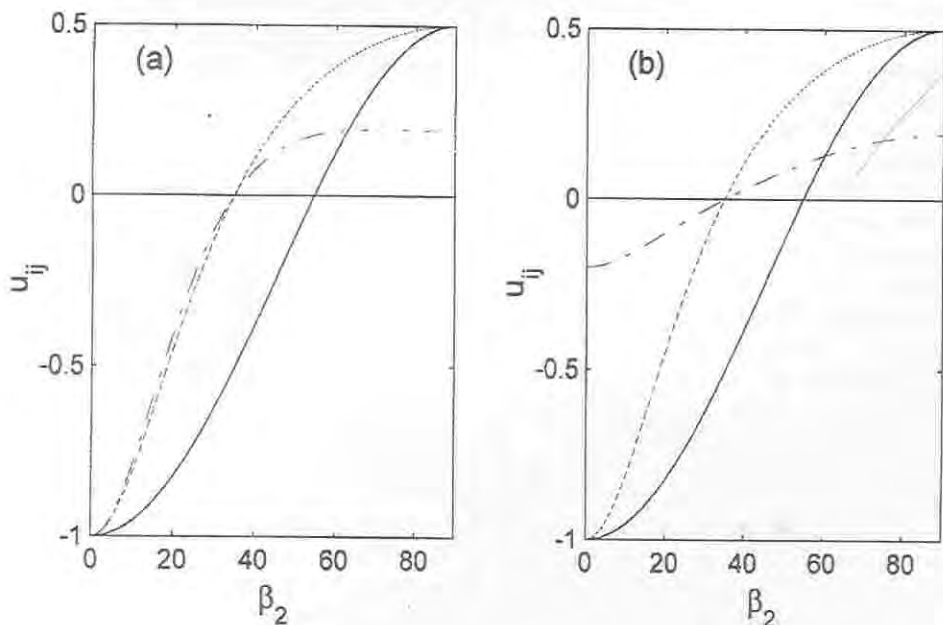


Figure 1. Comparison of the pair potentials of LL (solid line), BPAN (dotted line), and GBAN (dashed-dotted line) where  $\kappa = 5$ ,  $\kappa' = 5$ ,  $\alpha_1 = \alpha_2 = \beta_1 = \phi = 0$ ,  $\beta_2$  is varied and a)  $\theta = \pi/2$  (side-by-side configuration) and b)  $\theta = 0$  (end-to-end configuration).

Figure 1(a-b) show comparison of the plots of the pair potentials for LL (solid line), BPAN (dotted line) and GBAN (dashed-dotted line), where  $\kappa = 5$ ,  $\kappa' = 5$ ,  $\alpha_1 = \alpha_2 = \beta_1 = \phi = 0$ ,  $\beta_2$  is varied and a)  $\theta = \pi/2$  (side-by-side configuration) and b)  $\theta = 0$  (end-to-end configuration). Comparison of the dotted and solid lines in figures a and b shows how the LL potential is modified by including a parameter which controls the elongation of molecules. The effect of a parameter which controls the intermolecular vector orientation dependence on the pair potential is demonstrated by comparing the dotted and dashed-dotted lines in the two plots. The potential is drastically modified when a parameter which controls the intermolecular vector orientation dependence is included in the potential.

In Figure 2 (a-c) we shall compare the intermolecular vector polar angle  $\theta$  and the second molecule polar angle  $\beta_2$ , which is adjusted to be equivalent to  $\beta_{12}$ , dependence of the model pair potentials a) LL, b) BPAN, and c) GBAN where  $\kappa = 5$ ,  $\kappa' = 5$ ,  $\alpha_1 = \alpha_2 = \beta_1 = \phi = 0$ . The intermolecular vector orientation independence of LL and BPAN potentials are evident from Figures 2a and 2b where the potentials remained constant as  $\theta$  is varied. However, the peak appears to be sharper for BPAN due to its dependence on molecular elongation. Figure 2c shows the strong intermolecular vector orientation dependence of GBAN.

The comparison of the dependence of the three model pair potentials on the molecular elongation ( $\kappa = \sigma_l/\sigma_s$ ) and intermolecular vector orientation dependence parametrized via the potential strength anisotropy  $\kappa' = \epsilon_l/\epsilon_s$  is given in Figures 3(a-c). Comparison of the three plots show that the effect of the molecular elongation and intermolecular vector orientation dependence make the potential well depth shallower relative to that of LL. The effect of the molecular elongation parameter ( $\kappa = \sigma_l/\sigma_s$ ) appears to be much stronger than that of the potential well depth anisotropy parameter  $\kappa' = \epsilon_l/\epsilon_s$ .

The two parameters  $\mu$  and  $\nu$  in the well depth function take different sets of values without affecting the relative well depths for the side-by-side and end-to-end configurations (see for example in Table 2). However, their relative values affect the relative well depth for the end-to-end and T-configurations. If  $\mu \leq \nu$  the side-by-side configuration and end-to-end configuration are more stable than the cross and the T-configurations. Smectic systems are expected to be stabilized if the end-to-end configuration is stabilized relative to the T-configuration. However, the parametrization with  $\mu \leq \nu$  is not suitable for scaling. Figure 4 shows how end-to-end configuration can be stabilized relative to the T-configuration by properly tuning the relative values of the molecular elongation parameter ( $\kappa = \sigma_l/\sigma_s$ ) and intermolecular vector orientation dependence parametrized via the potential strength anisotropy  $\kappa' = \epsilon_l/\epsilon_s$ . The curve connects points where the well depth for the end-to-end configuration is equal to the cross and the T-configurations. For any value of  $\kappa' = \epsilon_l/\epsilon_s$  the well depth for the end-to-end configuration is deeper than that of the T-configuration above the curve and shallower below the curve. For the N-site per molecule Lennard-Jones potential the end-to-end configuration potential well depth is always shallower than that of the T configuration. The values for  $N = 4$  are compared in Table 2. A potential which can be tuned in such a way that the relative well depth for the end-to-end configuration, and T-configurations is of interest for studies of interfacial properties of mesogens preferring a perpendicular or a parallel orientation at the interface [10].



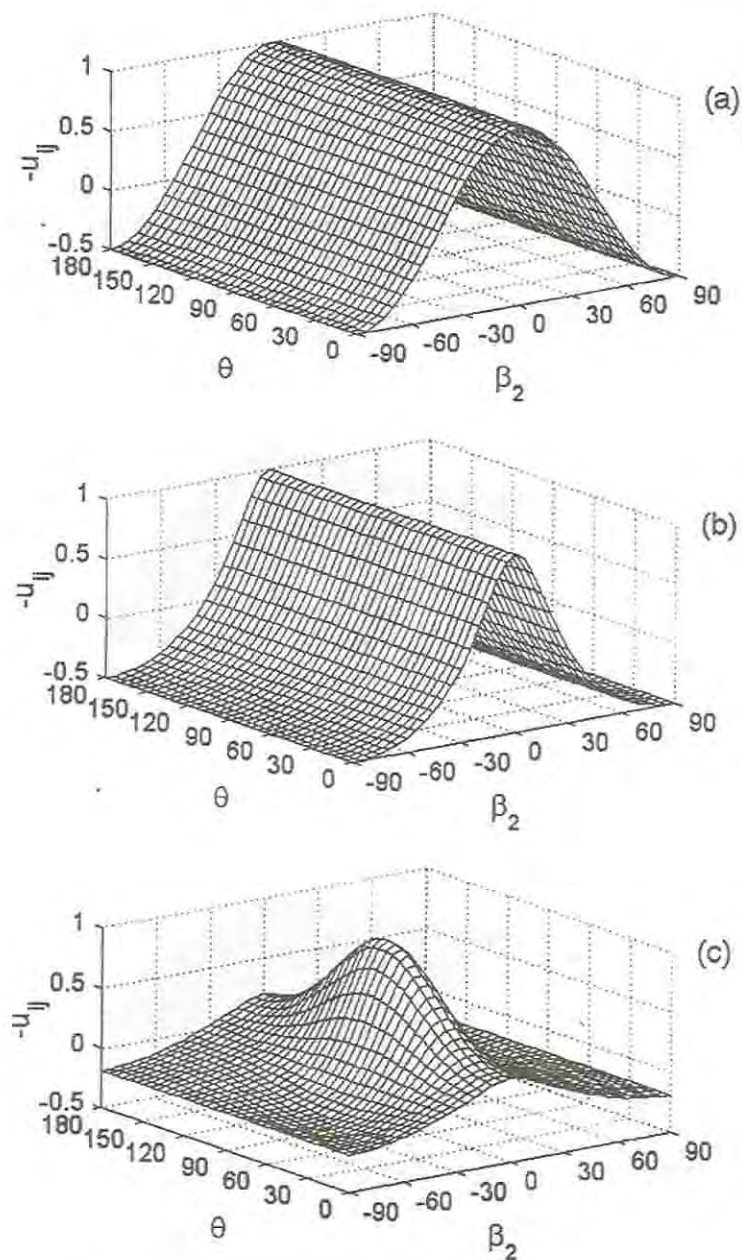


Figure 2. Comparison of the model pair potentials where  $\kappa = 5$ ,  $\kappa' = 5$ ,  $\alpha_1 = \alpha_2 = \beta_1 = \phi = 0$ , and the intermolecular vector polar angle  $\theta$  and the second molecule polar angle  $\beta_2$  (set up to be equivalent to  $\beta_{12}$ ) are varied. a) LL, b) BPAN, and c) GBAN

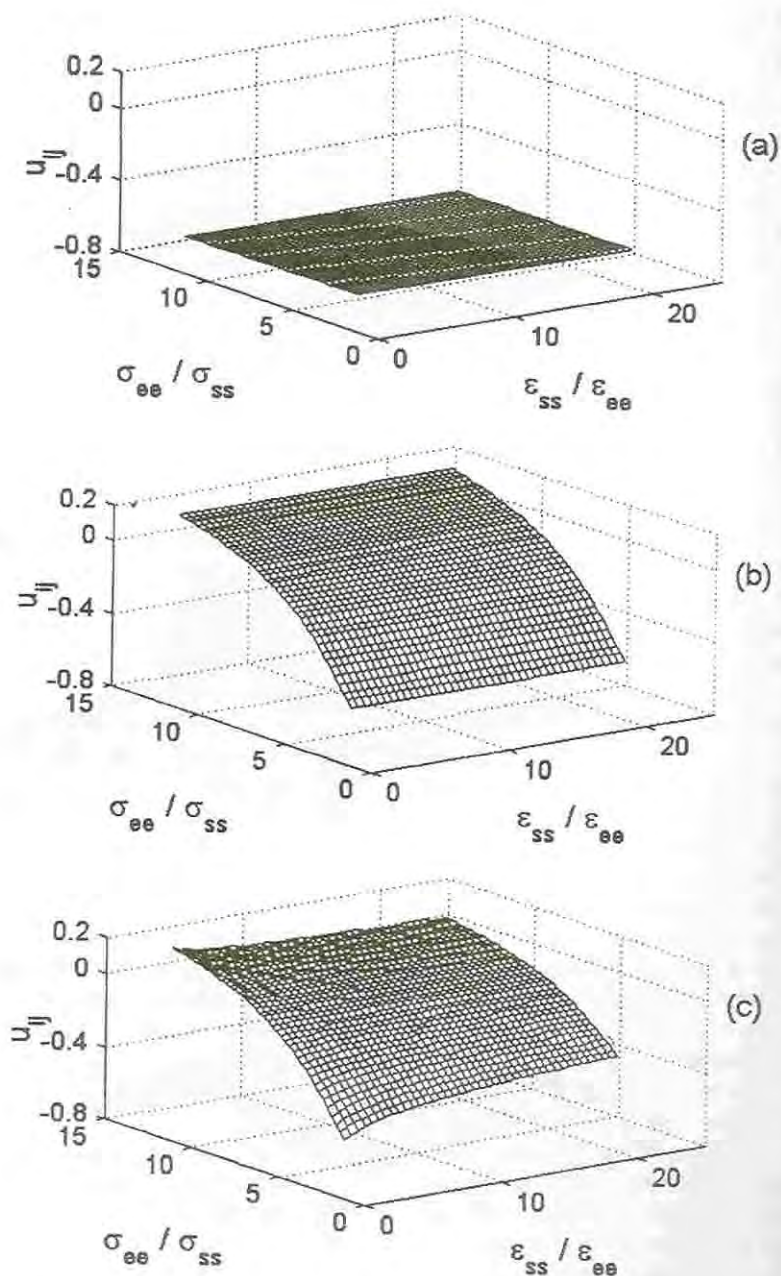


Figure 3. Comparison of the model pair potentials dependence on the molecular elongation ( $\kappa = \sigma_i/\sigma_j$ ) and intermolecular vector orientation dependence parametrized via the potential strength anisotropy  $\kappa = \epsilon_s/\epsilon_e$ . a) LL, b) BPA, and c) GBAN where  $\alpha_1 = \alpha_2 = \beta_1 = \phi = 0$ ,  $\beta_2 = 50^\circ$  and  $\theta = 90^\circ$ .



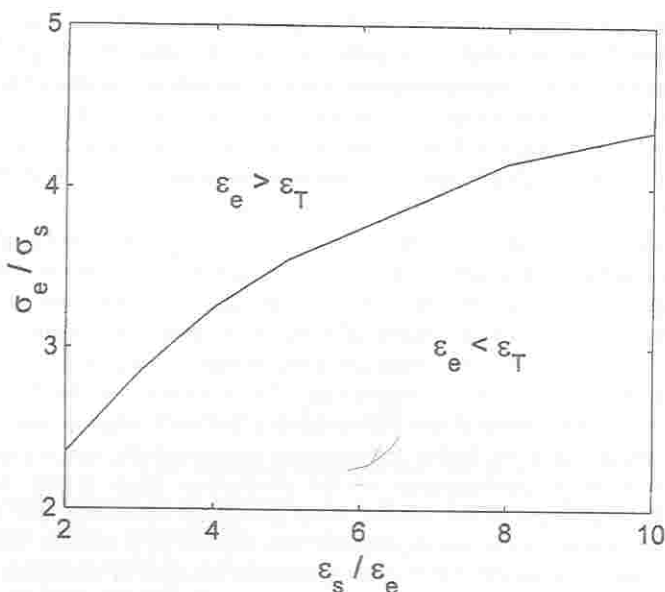


Figure 4. Plot showing the relative stabilities of end-to-end and side-by-side configurations as a function of the molecular elongation parameter ( $\kappa = \sigma_l/\sigma_\perp$ ) and intermolecular vector orientation dependence parametrized via the potential strength anisotropy  $\kappa' = \epsilon_s/\epsilon_e$ .

Table 2. Potential well depth for selected configurations: Cross ( $\epsilon_x$ ) used as scaling parameter, T ( $\epsilon_T$ ), Side-by-side ( $\epsilon_s$ ) and end-to-end ( $\epsilon_e$ ) for of the GB model and the four site Lennard-Jones rod (RLJ4).

v	$\mu$	$\kappa = \sigma_l/\sigma_\perp$	$\kappa' = \epsilon_s/\epsilon_e$	$\epsilon_s$	$\epsilon_e$	$\epsilon_T$	$\epsilon_x$
1	2	5	5	-2.6	-0.52	-0.382	-1
1	2	3	5	-1.66	-0.333	-0.38	-1
2	1	5	5	-6.76	-1.35	-0.333	-1
2	1	3	5	-2.77	-0.555	-0.333	-1
RLJ4				-1.15	-0.173	-0.42	-1

## COMPUTATIONAL DETAILS

In order to assess the changes in the thermodynamic and structural properties of a nematic which would result from the variation of parameters which control the length of molecules and the intermolecular vector orientation dependence in the pair potential we have carried out a detailed simulation. Extensive studies were made on a system of rod-like molecules with length-to-width ratio  $\sigma_l/\sigma_w$  equal to 3 and 5, and well depth anisotropy  $\kappa = \epsilon_l/\epsilon_w$  of 1, 3 and 5 and interacting with the GBAN potential. For comparison we also have generated the data for the LL and GBA models.

In this study we have chosen a simple cubic lattice of dimensions  $10 \times 10 \times 10$  where each lattice site is occupied by a single particle and interactions are restricted only to nearest neighbours. This is known to be sufficient to yield the structural and thermodynamic properties of simulated models as a function of temperature with a reasonable accuracy [34]. A standard Monte Carlo method of simulation with periodic boundary conditions has been employed to generate equilibrium configurations. The simulation at the first temperature studied for all the systems studied was started from a perfectly aligned state along the z-direction. The simulations at the higher temperatures were normally run in cascade starting from the last equilibrium configuration of the production stage at the nearest lower temperature. The trial orientational moves were generated following the Barker-Watts technique in which a particle chosen sequentially was rotated by a random amount about a laboratory axis selected at random [35]. The attempted changes in rotational moves were accepted following the standard Metropolis algorithm [36]. The acceptance ratio was checked and the maximum allowed changes, say  $\Delta$  corresponding to the maximum changes in orientations in radians was adjusted every macrocycle to be in the range 0.4 to 0.6. A cycle typically consists of a 1000 random attempted orientational moves and a macrocycle is typically 2500 cycles. Equilibration was monitored via the internal energy and order parameter sub-averaged over a macrocycle. Typically 10 macrocycles were generated for each temperature studied in the equilibration phase. After preparing a well equilibrated configuration, structural and thermodynamic properties were calculated. For all temperatures studied a minimum of  $2.5 \times 10^7$  configurations were generated for the production stage. Near the temperatures where we expected a phase transition to occur we performed longer runs. The statistical errors in the properties calculated were estimated by considering sub-averages of the properties over successive blocks of a macrocycle length for 10 macrocycles.

*Structural properties.* A complete microscopic description of the various mesophases can, in principle, be obtained in terms of molecular distribution functions. For most purposes the singlet and pair distributions are adequate. In general, distribution functions are not experimentally accessible. However, these distribution functions can be calculated by computer simulation. Experimentally liquid crystals are characterized by using various types of order parameters. These order parameters are defined as expansion coefficients of the singlet distribution function on a suitable basis set. Fourier series for position and Wigner series for orientation are used as the basis sets to define orientational, translational and mixed orientational-translational order parameters. For a linear molecule in a uniaxial phase with no translational order the single particle distribution function can be expanded as [1]

$$f(\beta) = \sum_L ((2L+1)/2) \langle P_L \rangle P_L(\cos\beta) \quad (11)$$

where  $P_L$  stands for the  $L^{\text{th}}$  rank Legendre polynomial and  $\beta$  is the angle between a molecule

and the director and the expansion coefficients  $\langle P_L \rangle$  are defined as

$$\langle P_L \rangle = \int P_L(\cos\beta) f(\cos\beta) d\cos\beta \quad (12)$$

The second rank order parameter,  $\langle P_2 \rangle$ , used to characterize pure orientational order is conveniently defined for evaluating by computer simulation as [8]

$$\bar{P}_2 = \left\langle (1/N) \sum_{i=1}^N P_2(\cos\beta_i) \right\rangle \quad (13)$$

where the angular brackets indicate ensemble averages,  $N$  is the number of particles and  $\beta_i$  is the angle between molecule  $i$  and the director.

The calculations of order parameters and some of the distribution functions require the knowledge of the director orientation. In computer simulations the director is not known *a priori* and it may fluctuate during the evolution of the system. In general the second rank orientational order parameter and the direction of the director for a given configuration can be calculated from a second rank tensor defined as [8]

$$Q_{\alpha\beta} = (1/N) \sum_{i=1}^N (1/2)(3u_\alpha^i u_\beta^i - \delta_{\alpha\beta}) \quad (14)$$

where  $u_\alpha^i$ ,  $\alpha = x, y, z$  is the direction cosine of the unit vector describing the  $i^{\text{th}}$  molecular orientation with respect to an arbitrary space fixed frame. At the temperatures where the configurations show considerable orientational order the fluctuations of the director orientation during a cycle is insignificant. Considering this slow fluctuation of the director orientation we have reduced the computational time by sampling the Q-tensor only once at the end of a cycle and accumulated for 30 to 50 consecutive cycles. The Q-tensor was then averaged and diagonalized. Its largest positive eigenvalue was collected and averaged to give the second rank orientational order parameter  $\langle P_2 \rangle$ . Whenever a director orientation was needed to calculate other structural properties the eigenvectors of the last Q-tensor diagonalized was determined and the one associated with the largest eigenvalue was identified with the director. Once the director orientation is located a variety of structural properties parallel and perpendicular to the director can be calculated. The frequency of the eigenvector determination depends on the frequency of sampling of structural properties which depends on the knowledge of orientation of the director.

In order to study the short-range order in the system in detail we have also calculated the second and fourth rank angular pair correlation functions. The angular pair correlation functions are defined as the expansion coefficients of the rotational invariant pair distribution function  $G(r_{ij}, \beta_{ij})$  which determines the probability of finding two particles separated by a distance  $r_{ij}$  with a certain relative orientation  $\beta_{ij}$ . It is convenient to expand  $G(r_{ij}, \beta_{ij})$  in a series of Legendre polynomial as [8]

$$G(r_{ij}, \beta_{ij}) = G_0(r_{ij}) \sum_L ((2L+1)/2) G_L(r_{ij}) P_L(\cos\beta_{ij}(r_{ij})), \quad L \text{ even} \quad (15)$$

where  $G_0(r_{ij})$  is the scalar distribution of the particles centre of mass and the expansion coefficients  $G_L(r_{ij})$  define two-particle order parameters. These in turn give the correlation between the orientation of two particles separated by a distance  $r_{ij}$  and are given as [8]

$$G_L(r_{ij}) = (1/G_0(r_{ij})) \int d\beta_{ij} G_L(r_{ij}, \beta_{ij}) P_L(\cos\beta_{ij}(r_{ij})) = \langle P_L(\cos\beta_{ij}(r_{ij})) \rangle, \quad L \text{ even} \quad (16)$$

For lattice systems the particle positions are fixed and their distribution is just a series of delta functions centred at the successive lattice sites at distance  $r/a_0$  from the reference particle and with a population of  $z(r/a_0)$  neighbours. In order to study the effect of the intermolecular vector orientation dependence on the pair angular correlation functions in the system we have also calculated the pair correlation functions perpendicular to the director  $G_L^+(r_\perp^*)$  and parallel to the director  $G_L^1(r_\parallel^*)$ . These structural properties are conveniently defined for evaluating by computer simulation as

$$G_L(r^*) = \left\langle (1/Nz(r^*)) \sum_{i=1}^N \sum_{j \neq i}^N P_L(\cos \beta_{ij}(r^*)) \delta(r^* - r_{ij}^*) \right\rangle \quad (17)$$

$$G_L^\perp(r_\perp^*) = \left\langle (1/Nz(r_\perp^*)) \sum_{i=1}^N \sum_{j \neq i}^N P_L(\cos \beta_{ij}(r_\perp^*)) \delta(r_\perp^* - r_{ij,\perp}^*) \right\rangle \quad (18)$$

$$G_L^1(r_\parallel^*) = \left\langle (1/Nz(r_\parallel^*)) \sum_{i=1}^N \sum_{j \neq i}^N P_L(\cos \beta_{ij}(r_\parallel^*)) \delta(r_\parallel^* - r_{ij,\parallel}^*) \right\rangle \quad (19)$$

where  $\delta$  is a delta function taken to be unity for  $\delta(0)$ , and zero otherwise. A histogram was compiled of all pair separations satisfying the conditions where  $r_{ij,\perp}^* = (|r_{ij}^*|^2 - \hat{n} \cdot \vec{r}_{ij}^*|^2)^{1/2}$  and  $r_{ij,\parallel}^* = \hat{n} \cdot \vec{r}_{ij}^*$ ,  $\delta(|r_{ij}^*| - |\hat{n} \cdot \vec{r}_{ij}^*|)$ .

## SIMULATION RESULTS AND DISCUSSION

*Internal energy.* The internal energies of the various systems studied is calculated as a sum of the pair interactions  $\langle U \rangle = (1/2) \langle \sum_i^N \sum_{\{ij\}} U_{ij} \rangle$ . The angular brackets imply ensemble average and the  $\{ij\}$  implies restriction on  $j$  to only the nearest neighbours of  $i$  and  $N$  is the number of particles. The temperature dependence of the scaled single particle energy  $\langle U \rangle / N\epsilon_0$  for the six systems studied is shown in Figure 5 (a-f). For a system expected to show a first order transition the internal energy is expected to show a discontinuity. In all the six cases studied the internal energy appears to vary continuously with temperature. This is due to the weak nature of the transition and the small number of particles employed in the simulation. However, the shape of the temperature dependence of the internal energy close to the transition varies as the elongation and potential well anisotropy parameters change. These changes qualitatively show how the transitional properties of the six systems vary as the two parameters change. The transition appears to get sharper as either of the parameters increases. The transition temperature appears to shift to lower values as either of the parameters are increased. A more definite location of the nematic-isotropic transition temperature can be identified from the temperature dependence of the heat capacity.

*Heat capacity.* It is known that the heat capacity is a very temperature sensitive property close to a phase transition. It shows a divergence, a discontinuity or a peak near a phase transition. It is, therefore, used to locate a transition temperature and characterize the order of the a transition. In computer simulation heat capacity can be obtained as a fluctuation of the internal energy  $C_V = (\langle \bar{U}^2 \rangle - \langle \bar{U} \rangle^2) / kT^2$ . Given the mean square and the square mean of the internal energy, in principle the heat capacity can be calculated. However, since  $C_V$  calculated in this way is actually obtained as a fluctuation quantity it is often prone to large errors and uncertainties. When the heat capacity show large error the other alternative is to do

numerical differentiation of the internal energy. It is known that the differentiation of experimental or, in general, noisy data is an ill-posed problem [34]. It can be tackled through smoothing interpolation, for example, using suitable spline functions. In Figure 6 (a-f) we present the temperature dependence of the heat capacity obtained via numerical differentiation of the internal energy with respect to temperature. Comparing the various curves we see that the heat capacity becomes more divergent and the peak position shifts to lower temperatures as either of the two parameters increases. Tables 3 and 4 summarize the position of the heat capacity maxima,  $T_{NI}$  and the dependence of the heat capacity maxima as a function of the two parameters, molecular elongation parameter  $\kappa = \sigma_v/\sigma_\perp$  and potential well depth anisotropy parameter  $\kappa' = \epsilon_s/\epsilon_e$ .

Table 3.  $kT_{NI}/\epsilon_0$  for various systems with different values of molecular elongation parameter  $\kappa = \sigma_v/\sigma_\perp$  and potential well depth parameter  $\kappa' = \epsilon_s/\epsilon_e$ .

$\kappa = \sigma_v/\sigma_\perp$	1	3	3	3	5	5	5
$\kappa' = \epsilon_s/\epsilon_e$	1	1	3	5	1	3	5
$kT_{NI}/\epsilon_0$	1.127	1.05	0.78	0.703	0.94	0.695	0.627
$\bar{P}_2^{NI}$	0.328	0.43	0.382	0.351	0.46	0.423	0.42

Table 4. Comparison of results obtained from various potential models on the thermodynamic properties of the nematic-isotropic phase. Here, LLI: Inhomogeneous Lebwohl-Lasher, BPAN: normalized angular part of Berne-Pechukas, GBAN: normalized potential derived from Gay-Berne and GBA potential derived from that of Gay-Berne. Here  $\uparrow$  and  $\uparrow\uparrow$  indicates increasing and strongly increasing trends, respectively, NA indicates not available and C stands for a constant.

			$kT_{NI}/\epsilon_0$	$P_2^{NI}$	$ dP_2/dT^* _{MAX}$	$C_{V,MAX}/Nk$
LLI [34]	$\delta$	$\downarrow$	$\downarrow$	NA	$\uparrow$	$\downarrow$
BPAN [20]	$\kappa = \sigma_v/\sigma_\perp$	$\uparrow$	$\downarrow$	$\uparrow$	NA	$\uparrow$
GBAN	$\kappa = \sigma_v/\sigma_\perp$	$\uparrow$	$\downarrow$	$\uparrow$	$\uparrow\uparrow$	$\uparrow\uparrow$
	$\kappa' = \epsilon_s/\epsilon_e$	$\uparrow$	$\downarrow$	$\downarrow$	$\uparrow$	$\uparrow$
GBA	$\kappa = \sigma_v/\sigma_\perp$	$\uparrow$	$\uparrow$	$\downarrow$	$\uparrow$	$\uparrow$
	$\kappa' = \epsilon_s/\epsilon_e$	$\uparrow$	$\uparrow$	$\uparrow$	$\uparrow$	$\uparrow$
HLR [26]	$\gamma$	$\uparrow$	C	C	NA	$\uparrow$



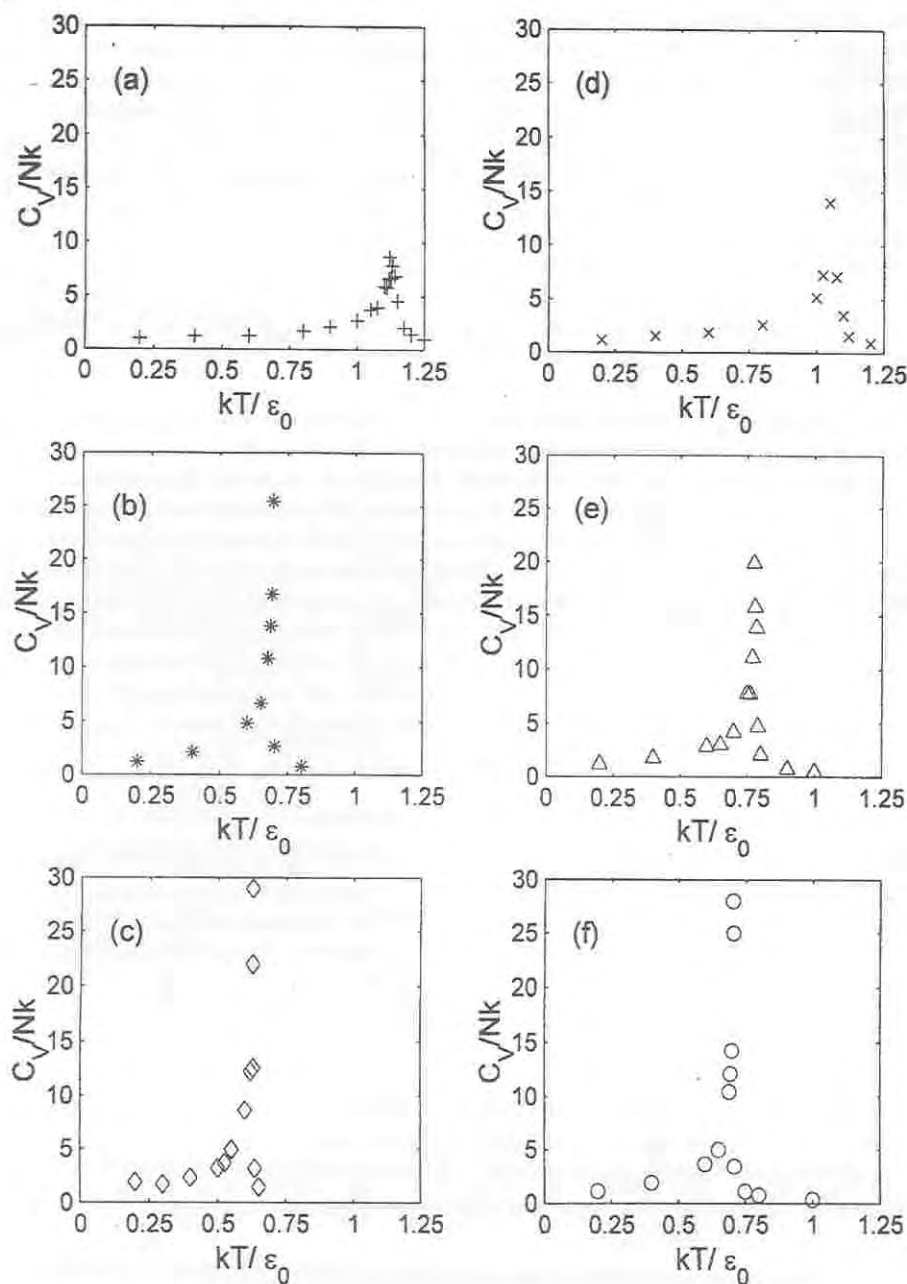


Figure 6. The scaled heat capacity per particle  $C_v/Nk$  shown as a function of reduced temperature for the LL model (a) and GBAN model (b-f). a) LL model, b)  $\kappa = 5$  and  $\kappa' = 3$ , c)  $\kappa = 5$  and  $\kappa' = 5$ , d)  $\kappa = 3$  and  $\kappa' = 1$ , e)  $\kappa = 3$  and  $\kappa' = 3$ , f)  $\kappa = 3$  and  $\kappa' = 5$ .

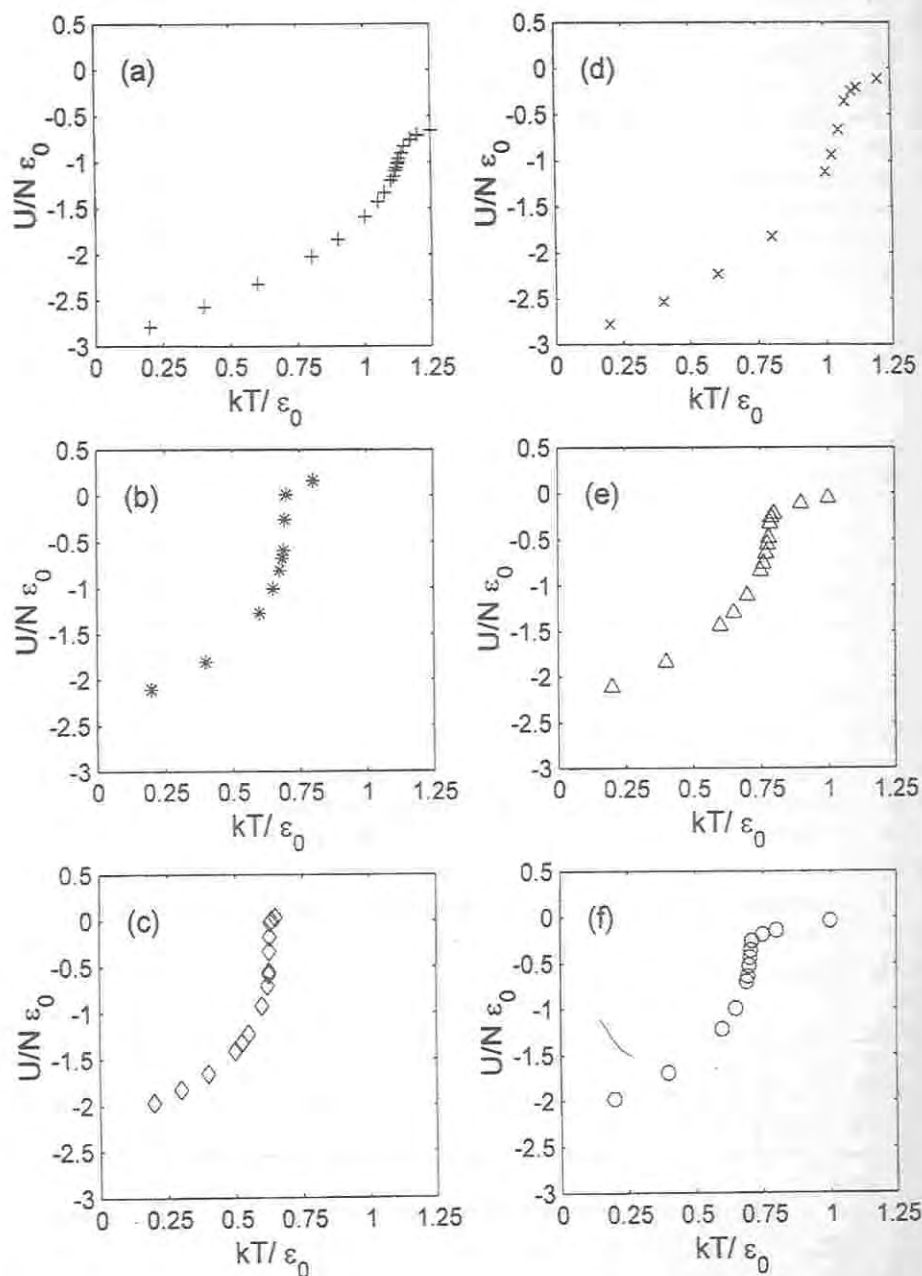


Figure 5. The scaled internal energy per particle  $\langle U/N\epsilon_0 \rangle$  shown as a function of the reduced temperature  $kT/\epsilon_0$  for the LL model (a) and GBAN model (b-f). a) LL model, b)  $\kappa = 5$  and  $\kappa' = 3$ , c)  $\kappa = 5$  and  $\kappa' = 5$ , d)  $\kappa = 3$  and  $\kappa' = 1$ , e)  $\kappa = 3$  and  $\kappa' = 3$ , f)  $\kappa = 3$  and  $\kappa' = 5$ .

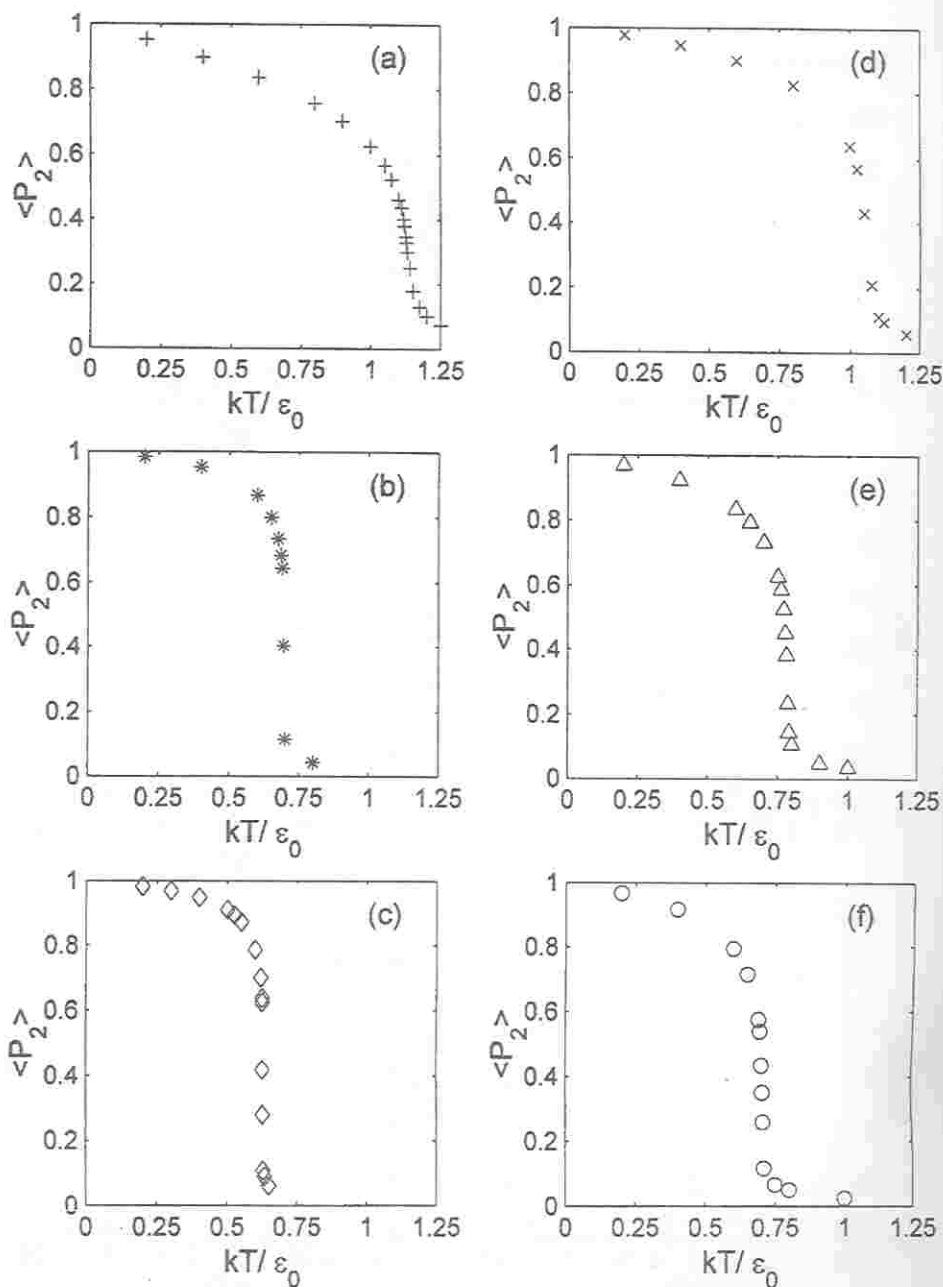


Figure 7. Plots of the second rank orientational order parameters as a function of the scaled temperature for the LL model (a) and GBAN model (b-f). a) LL model, b)  $\kappa = 5$  and  $\kappa' = 3$ , c)  $\kappa = 5$  and  $\kappa' = 5$ , d)  $\kappa = 3$  and  $\kappa' = 1$ , e)  $\kappa = 3$  and  $\kappa' = 3$ , f)  $\kappa = 3$  and  $\kappa' = 5$ .

*Second rank orientational order parameter.* The temperature dependence of the order parameter  $\langle P_2 \rangle$  for the six systems studied is shown in Figure 7(a-f). The order parameter is seen to vary continuously with temperature and does not fall to the value of zero expected for the isotropic phase and this behaviour is attributed to the relatively small number of particles employed in the simulation. In order to quantify the rate of fall of the order parameter with temperature we have performed a numerical differentiation. In all cases studied the temperature at which the heat capacity is maximum coincided with that at which the derivative of the order parameter is maximum. This makes the transition temperature identified via the two different routes identical. The rate of change of the order parameter with temperature close to the nematic isotropic transition gets higher as either of the parameters increases. This fast rate of change of the order parameter makes determination of the nematic order parameter at the transition  $P_2^{Ni}$  difficult. However, we are able to estimate  $P_2^{Ni}$  as the one at the transition temperature identified by the position of the heat capacity peak. The results are summarized in Table 3. It is observed that the order parameter at the transition decreases as the potential well anisotropy parameter increases for a fixed molecular elongation parameter. However, this trend is reversed for the case of molecular elongation. The order parameter at the transition increases as molecular length increases at fixed potential well depth parameter increases. These results are summarized in Table 4.

Similar thermodynamic and structural properties of different systems which are universal functions of the reduced temperature are expected to fall on the same curve. The simulation results for the order parameter as a function of the reduced temperature  $T/T_{Ni}$  for the six systems studied are compared in Figure 8. For the sake of comparison of the simulation results with the predictions of the simple mean field theory we chose the inhomogeneous Lebwohl-Lasher model (LLI). In the LLI model the potential of mean torque is given by [34]

$$U(\beta) = -\epsilon_{\perp}(2\delta + 4)\langle P_2 \rangle P_2(\cos\beta) \quad (20)$$

where  $\beta$  is the angle between a molecule and the director,  $\epsilon_{\perp}$  is the strength of the attractive interactions perpendicular to the director,  $\delta$  is the ratio of the parallel to the perpendicular attractive interaction strength parameters which might be loosely compared to  $1/\kappa'$  of the GB potential well anisotropy parameter and  $\langle P_2 \rangle$  is the second rank order parameter obtained by numerical solution of the self consistent field equation

$$\langle P_2 \rangle = \frac{\int P_2(\cos\beta) e^{-U(\beta)/kT} d\cos\beta}{\int e^{-U(\beta)/kT} d\cos\beta} \quad (21)$$

At the molecular field theory level the effect of changing the interlayer coupling  $\delta$  is merely re-normalizing the isotropic-nematic transition temperature. The character of the transition remains unchanged as  $\delta$  is varied. All the transitional properties are predicted to be insensitive to  $\delta$ . The simple meanfield theory also predicts  $\langle P_2 \rangle$  to be a universal function of  $T/T_{Ni}$ .

In Figure 8 the simulation results are compared against predictions of the simple molecular field theory. The solid curve represents the prediction of the mean field theory for the temperature dependence of  $\langle P_2 \rangle$  for any finite value of  $\delta$  and the points are results of the simulation. The simulation results appear to fall into three universal curves. Each curve is characterized by the shape anisotropy parameter: the first group being the predictions of the mean field theory (solid curve) and that of the LL model this is characterized by the shape anisotropy parameter  $\kappa = 1$  (+), the second group which fall on the same curve are the

simulation results for the three GBAN models  $\kappa = 3$  and  $\kappa' = 1(x)$ ,  $\kappa' = 3(\Delta)$ ,  $\kappa' = 5(*)$ , and the third group is the simulation results for the two GBAN models with  $\kappa = 5$  and  $\kappa' = 3(o)$ ,  $\kappa' = 5(\diamond)$ . The reduced temperature dependence of the order parameter seems to be more sensitive to the molecular elongation parameter than the potential well depth anisotropy parameter which appears to show minor variations. It is well known that  $\langle P_2 \rangle$  for real systems is not a universal function of the reduced temperature[1]. The variation in the reduced temperature dependence of the order parameter of the different systems seems to be addressed with the GBAN model by varying simply the elongation and potential well anisotropy parameters. The molecular field theory predicts order parameter and transitional properties which looks like experimental results or that of the simulation results by introducing at least a two order parameter theory: including a fourth rank interaction in the potential of mean torque [26]

$$U(\beta) = -\epsilon_0 \{ \langle P_2 \rangle P_2(\cos\beta) + \lambda \langle P_4 \rangle P_4(\cos\beta) \} \quad (22)$$

where  $\lambda$  is a measure of the relative importance of the fourth rank term to the second rank term or by introducing molecular biaxiality as there are more compelling reasons to justify the inclusion of terms in the pair potential to allow for deviations from molecular cylindrical symmetry. This can easily be seen from the structures of PAA, MBBA and the idealized prolate ellipsoid used to represent the molecules which is given in Table 1. The lack of molecular symmetry may not preclude the possibility that the pair potential is effectively that for cylindrical particles because the terms which result from deviations from cylindrical symmetry may be small.

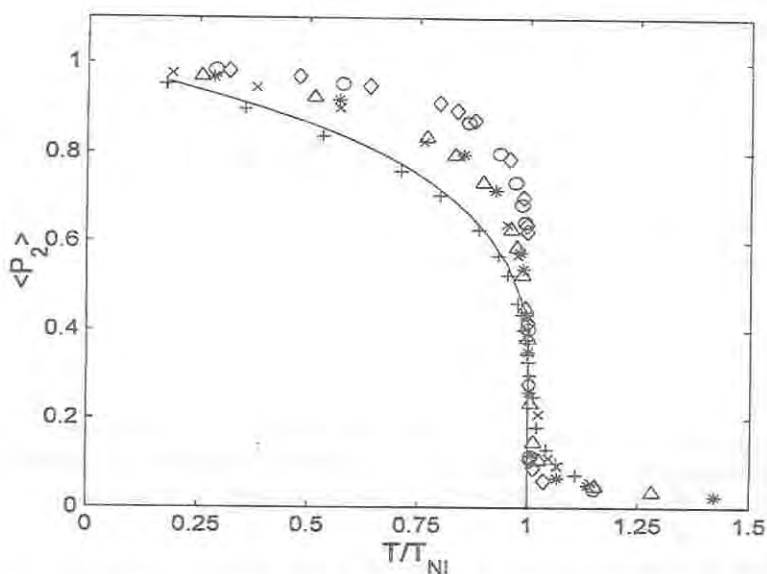


Figure 8. Plot of the second rank order parameters as a function of the reduced temperature  $T/T_{NI}$  for the simple mean field theory (solid line) for the LL model (+), and GBAN model  $\kappa = 3$  and  $\kappa' = 1(x)$ ,  $\kappa' = 3(\Delta)$ ,  $\kappa' = 5(*)$ , and  $\kappa = 5$  and  $\kappa' = 3(o)$ ,  $\kappa' = 5(\diamond)$ .



Table 4 summarizes the results on the transitional properties of the various model potentials as a function of the potential parameters.  $P_2^{NI}$  is the value of the order parameter at  $T_{NI}$  which is identified with the position of  $C_{V,MAX}$ .  $P_2^{NI}$  increases with  $\kappa$  for both BPAN and GBAN. However, it decreases as  $\kappa'$  increases for GBAN. It is interesting to observe that the transitional properties of a system can change by scaling the potential.  $P_2^{NI}$  increases for GBAN while it decreases for GBA as  $\kappa$  increases. An opposite trend is observed for the transition temperature. The heat capacity and derivative of the order parameter maximum increases for BPAN, GBAN and GBA as both  $\kappa$  and  $\kappa'$  increases. The effect of  $\kappa$  on the maximum of the order parameter maximum and that of the heat capacity is stronger for the case of GBAN. However,  $T_{NI}$  and  $P_2^{NI}$  appear to be insensitive to  $\gamma$  for the case of HLR model while  $C_{V,MAX}$  increases with  $\gamma$ . A decrease in  $\delta$  for LLI model is related to an increase in  $\kappa'$  in the GB model. The transition temperature decreases as  $\delta$  decreases and increasing  $\kappa'$  shows the same trend in LLI and GBAN. However, the heat capacity maximum shows opposite trend.

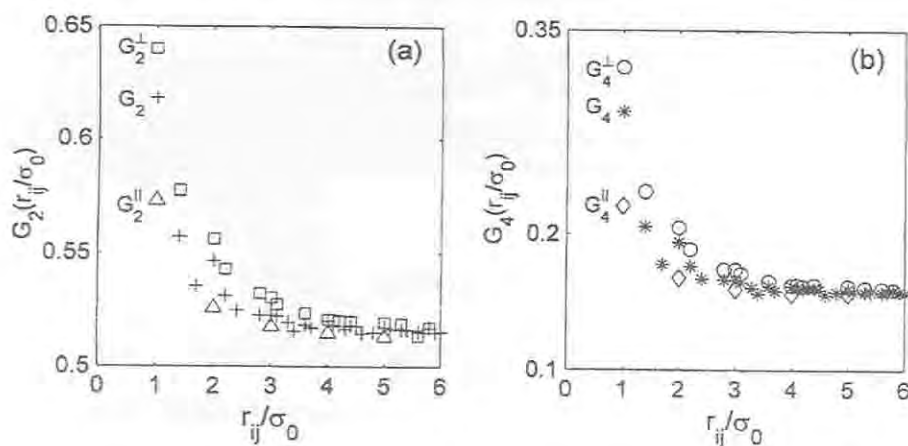


Figure 9. Plots of the first two angular pair correlation functions  $G_2(r)$  and  $G_4(r)$  at  $T^* = 0.65$  for the GBAN system with  $\kappa = 3$  and  $\kappa' = 5$ . a)  $G_2(r^+)$  (+),  $G_2(r_1^+)$  ( $\Delta$ ) and  $G_2(r_2^+)$  ( $\square$ ) and b)  $G_4(r^+)$  ( $\circ$ ),  $G_4^+(r_1^+)$  ( $\diamond$ ) and  $G_4^+(r_2^+)$  (\*).

*Angular pair correlation functions.* The simulation results for the first two angular pair correlation coefficients  $G_2(r/a_0)$  and  $G_4(r/a_0)$  obtained from simulation via equations (17-19) are presented in Figure 9(a-b). The figures compare the angular pair correlation function  $G_L(r/a_0)$  with those calculated parallel to the director  $G_L^+(r/a_0)$  and perpendicular to the director  $G_L^-(r/a_0)$  for  $L$  equal to 2 and 4 at  $T^* = 0.65$  for the GBAN ( $\kappa = 3$  and  $\kappa' = 5$ ). For both correlation functions the general trend is  $G_L^-(r/a_0) > G_L(r/a_0) > G_L^+(r/a_0)$ . This difference in the extent of angular correlation between  $G_L^-(r/a_0)$ ,  $G_L(r/a_0)$  and  $G_L^+(r/a_0)$  is very significant only between nearest neighbours. The effect of the intermolecular vector orientation dependence of the potential on the angular correlations dramatically decreases at the next nearest neighbours and vanishes beyond  $r/a_0 = 3$  for  $G_2(r/a_0)$  and  $r/a_0 = 2$  for  $G_4(r/a_0)$  and settles to their long-range values of  $\langle P_2 \rangle^2$  and  $\langle P_4 \rangle^2$ , respectively.

## CONCLUSIONS

We have proposed a modified Lebwohl-Lasher model of elongated molecules interacting via a potential derived from the Gay-Bern potential. The standard Metropolis Monte Carlo algorithm was used to simulate the system. Behaviour of the internal energy, heat capacity, order parameter and angular pair correlation functions were investigated. As compared to pure LL and modified Berne-Pechukas model both parameters of molecular elongation and intermolecular vector orientation dependence are present and the influence of these parameters on the phase transition is investigated. Simulation for the six cases showed unambiguously that nematic isotropic transition become more stronger first order one with increasing of either of the parameters. Comparing our results with the experimental data show that the thermodynamic and structural properties of many real nematics can be described well by the proposed model with elongation of molecules and potential well anisotropy parameters ranging from 3 to 5. Intermolecular vector orientation dependent potential is valuable for studies of interfacial properties and chiral nematic. Work in this direction is in progress.

## ACKNOWLEDGMENTS

The author acknowledges the Addis Ababa University Research and Publication Office (RPO) and School of Graduate Studies for financial support to purchase a PC and a Workstation.

## REFERENCES

1. Luchurst, G.R.; Gray, G.W. (Ed.) *The Molecular Physics of Liquid Crystals*, Academic Press: London; 1979.
2. Priestly, E.B.; Wojtowicz, P.G.; Sheng, P. (Ed.) *Introduction to Liquid Crystals*, Plenum Press: New York; 1979.
3. de Gennes, P.G. *The Physic of Liquid Crystals*, Oxford University Press: London; 1975.
4. Komolkin, A.V.; Molchanov, Y.V.; Yakusteni, P.P. *Liquid Crystals* **1989**, 6, 39.
5. Wilson, M.R.; Allen, M.P. *Molec. Cryst. Liq. Cryst.* **1991**, 198, 465.
6. Wilson, M.R.; Allen, M.P. *Liq. Cryst.* **1992**, 12, 157.
7. Lebwohl, P.A.; Lasher, G. *Phys. Rev. A* **1972**, 6, 426.
8. Zannoni, C. *The Molecular Physics of Liquid Crystals*, Luckhurst, G.R.; Gray, G.W. (Ed.), Academic Press: London; 1979; Chs. 3 and 9.
9. Luckhurst, G.R.; Romano, S. *Proc. R. Soc. Lond. A* **1980**, 373, 111.
10. Luckhurst, G.R.; Romano, S.; Zewdie, H.B. *J. Chem. Soc. Faraday Trans.* **1996**, 92, 1781.
11. Luckhurst, G.R.; Sluckin, T.J.; Zewdie, H.B. *Molec. Phys.* **1986**, 59, 657.
12. Eppanga, R.; Frenkel, D. *Molec. Phys.* **1984**, 52, 1303.
13. Frenkel, D. *J. Phys. Chem.* **1988**, 92, 3280.
14. Paolini, G.A.; Ciccotti, G.; Ferrario, M. *Molec. Phys.* **1993**, 80, 297.
15. Aoki, K.M.; Yonezawa, F. *Phys. Rev. A* **1992**, 46, 6541.
16. Berne, B.J.; Pechukas, P.J. *J. Chem. Phys.* **1972**, 56, 4213.
17. Gay, J.G.; Berne, B.J. *J. Chem. Phys.* **1981**, 74, 3316.
18. Zewdie, H. *J. Chem. Phys.* **1998**, 108, 2117.

19. Zewdie, H.. *Phys. Rev. E* **1998**, *57*, 1793.
20. Ilnytskyi, J.M. *Molec. Cryst. Liquid Cryst.* **1998**, *323*, 113.
21. Ilnytskyi, J.M.; Sokolwski, S. *Phys. Rev. E* **1999**, *59*, 4161.
22. Domb, C.; Green, M.S. *Phase Transitions and Critical Phenomena*, Oxford University Press: London; 1972.
23. Luckhurst, G.R.; Romano, S.; Simpson, P. *Chem. Phys.* **1982**, *73*, 337.
24. Fabbri, U.; Zannoni, C. *Molec. Phys.* **1986**, *59*, 763.
25. Haller, I. *Progr. Sol. St. Chem.* **1975**, *10*, 103.
26. Humphries, R.L.; Luckhurst, G.R.; Romano, S. *Molec. Phys.* **1981**, *42*, 1205.
27. Adams, D.J.; Luckhurst, G.R.; Phippen, R.W. *Molec. Phys.* **1987**, *61*, 1575.
28. Luckhurst, G.R.; Stephens, R.A.; Phippen, R.W. *Liquid Crystals* **1990**, *8*, 451.
29. Chalam, M.K.; Gubbins, K.E; de Miguel, E; Rull, L.F. *Molecular Simulation* **1991**, *7*, 357.
30. de Miguel, E.; Rull, L.F.; Chalam, M.K.; Gubbins, K.E.; van Swol, F. *Molec. Phys.* **1991**, *72*, 593.
31. de Miguel, E.; Rull, L.F.; Chalam, M.K.; Gubbins, K.E. *Molec. Phys.* **1991**, *74*, 405.
32. Berardi, R.; Emerson, A.P.J.; Zannoni, C. *J. Chem. Soc. Faraday Trans.* **1993**, *89*, 4069.
33. Hashim, R.; Luckhurst, G.R.; Romano, S. *J. Chem. Soc. Faraday Trans.* **1995**, *91*, 2141.
34. Chiccoli, C.; Pasini, P.; Zannoni, C. *Liquid Crystals* **1987**, *2*, 39.
35. Barker, J.A.; Watts, R.O. *Chem. Phys. Lett.* **1969**, *3*, 144.
36. Metropolis, N.; Rosenbluth, A.W.; Rosenbluth, M.N.; Teller, A.H.; Teller, E. *J. Chem. Phys.* **1953**, *21*, 1087.